Letter

Dissociation of red blood cell aggregates in extensional flow

Midhun Puthumana Melepattu,* Guillaume Maîtrejean,† and Thomas Podgorski‡
Université Grenoble Alpes, CNRS, Grenoble INP, LRP, 38000 Grenoble, France

(Received 4 March 2024; accepted 11 July 2024; published 29 July 2024)

Blood rheology and microcirculation are strongly influenced by red blood cell aggregation. We investigate the dissociation rates of red cell aggregates in extensional flow using hyperbolic microfluidic constrictions and image analysis by a convolutional neural network (CNN). Our findings reveal that aggregate dissociation increases sharply when a critical extension rate is reached which falls within the range of microcirculatory conditions, suggesting that large variations of aggregate sizes should be expected *in vivo*. This work contributes to a deeper understanding of the behavior of red blood cell aggregates in response to extensional stress in microcirculatory networks, provides crucial experimental data to validate theoretical and numerical models, and constitutes the basis for improved evaluation of blood aggregability in clinical contexts.

DOI: 10.1103/PhysRevFluids.9.L071101

Introduction. Plasma proteins, mainly fibrinogen, are responsible for a reversible aggregation of red blood cells (RBCs) [1]: near stasis and under low hydrodynamic stresses, the flat equilibrium shape of RBCs promotes their aggregation into clusters called "rouleaux " that resemble stacks of coins, eventually interconnecting to form 3D networks. As hydrodynamic stresses rise and overcome aggregation forces, the disaggregation of these structures, along with RBC deformability, results in the well-known shear-thinning behavior of blood [2]. Aggregation directly affects blood sedimentation, forming the basis of the erythrocyte sedimentation rate (ESR) test, a nonspecific inflammation marker [3].

Two mechanisms of aggregation have been identified. A bridging mechanism was proposed, supported by the evidence of macromolecule adsorption on the surface of RBCs and the role of electrostatic forces [4] to explain the nonmonotonous nature of the interaction force as a function of the macromolecular concentration. Both specific [5] and nonspecific [6,7] ligand interaction models have emerged. A second mechanism is based on depletion effects [8,9] due to the finite size of macromolecular aggregation promoters such as fibrinogen or dextran. While evidence shows that both mechanisms coexist in experimental situations, there are still open questions regarding their relative weight, depending on conditions (concentrations, synergies between fibrinogen and other factors, dextran of model experiments, alterations of the RBC membrane, etc.).

While shear rates in blood circulation are usually above 100 s^{-1} [10,11], a range where no influence of aggregation is detected in macroscopic rheology measurements [2], several works have revealed that aggregation interactions determine the structure of RBC suspensions in small channels [12,13], stabilize clusters in capillaries [14], or influence blood perfusion in networks [15]. A prominent feature of blood microcirculation is the heterogeneity of hematocrit distribution, a consequence of the Zweifach-Fung effect leading to an uneven distribution of RBCs at bifurcations,

*Contact author: Midhun.Puthumana-Melepattu@univ-grenoble-alpes.fr
†Contact author: Guillaume.Maitrejean@univ-grenoble-alpes.fr
‡Contact author: Thomas.Podgorski@univ-grenoble-alpes.fr

generally resulting in an increased hematocrit in the downstream branch with the highest flow [16–18]. While studies have focused on the influence of aggregation on hematocrit distribution, albeit in relatively wide channels [19,20], the stability of RBC aggregates in bifurcations has seldom been explored [21], although it is a strong determinant of aggregate size distribution in capillary networks. Indeed, aggregates evolve only slowly in straight channels or capillaries [14,22] and the distance between bifurcations is short *in vivo* [23]. On the other hand, significant extensional stresses in bifurcations of the microcirculation may control aggregate dissociation and size distribution.

Several studies, mostly computational, investigated the aggregation and dissociation dynamics of RBCs in shear flows [5,24] and associated rheological consequences [25]. This configuration is relevant to blood dynamics in large vessels down to arterioles or venules but not so much to circulation in capillaries where the confinement of RBCs and clusters is such that shear does not significantly affect aggregates. In contrast, their behavior in generic extensional flows, relevant in microcirculation scenarios with significant extensional stresses at bifurcations, has been rarely studied. Indeed, while bifurcations vary a lot *in vivo* (bifurcation angle, relative diameters and flow rates in branches), they share a localized strong extensional component of the stress tensor, prompting a need for understanding aggregate behavior in such conditions. In addition, extensional flows offer an alternative to costly and time consuming techniques like atomic force microscopy (AFM) [26] for quantifying aggregation forces or energy at the cellular level.

In this work, we provide a quantitative experimental study of RBC disaggregation in extensional flows using microfluidic hyperbolic constrictions. We focus on the impact of aggregation strength and flow extension stress on dissociation probabilities, proposing a straightforward scaling law. Our findings enhance comprehension of red blood cell aggregate behavior in microcirculatory networks, offering crucial experimental data for numerical model comparison and benchmarking. The proposed experimental principle, which can readily be used to study aggregate dissociation with RBCs in their own plasma rather than in dextran solutions, provides a high-throughput detailed measurement of the distribution of aggregate stability in a blood sample and an indirect measurement of interaction strength thanks to the proposed scaling law. This could form the basis of a RBC aggregability measurement that would complement existing techniques.

Experiment. The central part of the microfluidics setup is a hyperbolic constriction [Fig. 1(a)] producing a nearly planar extensional flow thanks to a decreasing channel width $w(x) \sim 1/x$, where x is the coordinate in the flow direction, as implemented in other works [27,28]. Results presented here were obtained using $w(0) = 200$ μm, $w(L) = 20$ μm, and a thickness $h = w(L)$ in the z direction and $L = 250$ μm. Mass conservation implies that the cross-sectional average of the axial velocity $\langle u_x(x) \rangle$ increases linearly along x, i.e., the average extension rate $d < u_x(x) > /dx$ is constant. Given that the Reynolds number $\mathrm{Re} = \rho v(L) h/2\eta$ (where ρ and η are the density and viscosity of the suspending fluid) is below 1 in all experiments and assuming that the velocity along the central axis $v_x(x) = u(x, 0, 0)$ increases linearly as the average velocity, a fluid particle flowing along the centerline will experience a nearly constant fluid extension rate defined as $\dot{\varepsilon_f} = dv_x/dx$. COMSOL numerical simulations were performed to confirm the quasilinearity of the velocity profile (see the Supplemental Material [29]).

In practice, the channel features a succession of constrictions with fixed inlet and outlet widths $w(0) = 200$ μm, $w(L) = 20$ μm, and decreasing lengths $L = 1000, 500, 250, 125$ μm exposing clusters to increasing extension rates. Each of them is followed by a straight channel [cross section $w(L) \times h = 20 \times 20$ μm^2, length 150 μm] in order to facilitate image acquisition at the end of the extensional flow region, and a large channel section ($w = 200$ μm, $L = 150$ μm) ensuring that clusters are relaxed before entering the next constriction. Note that due to strong confinement in the z direction, the average shear rate is actually quite high and of order $\dot{\gamma} \sim 2v_x(x)/h$, meaning that $\dot{\gamma}/\dot{\varepsilon_f} \sim 25$ at the end of the constriction. However, as already seen in previous works [14,22], in this configuration where flowing RBC aggregates are well centered in the channel the symmetric shear forces do not significantly contribute to disaggregation. Therefore, we expect extensional stresses to provide the dominant dissociation mechanism, which is confirmed by our observations below.

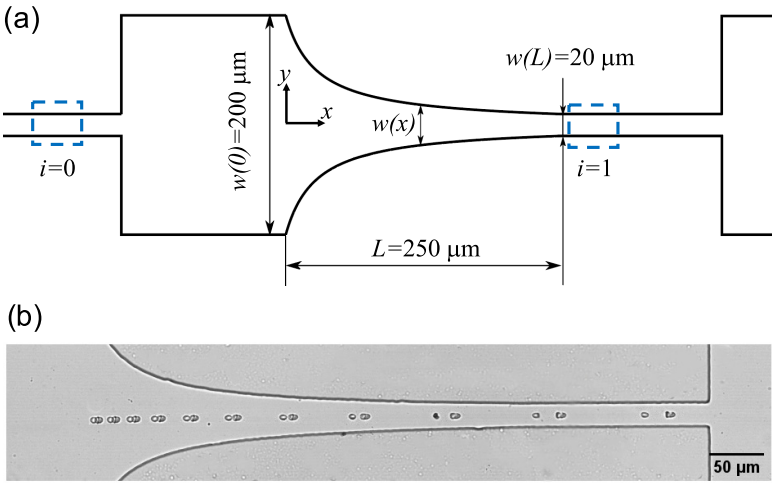

FIG. 1. Hyperbolic flow geometry producing extensional flow: (a) Design of the central part of the microfluidic channel and notations. Blue areas: image processing regions of interest (ROIs). (b) Example temporal sequence of a three-cell aggregate breaking into 2 + 1 cells in the extensional flow with $\dot{\varepsilon} = 204\ \mathrm{s}^{-1}$ (time step: 4 ms; dextran concentration 3 g/dL).

Blood samples provided through an agreement for the transfer of non-therapeutic blood products with the French Blood Establishment (EFS) (Ref. EFS AURA 22-082) were collected from healthy donors and anticoagulated with citrate, stored at 4 °C and used within 1 week after collection for consistent results [30]. A total of seven samples from different donors were used in the presented results. Before experiments, RBCs were washed by successive dilutions with phosphate buffered saline (PBS, Sigma-Aldrich, P4417) and centrifugations (1000 g × 3 min, three times). Aggregation was controlled by resuspending RBCs at an initial hematocrit of 2–3% in PBS supplemented with dextran 70 kDa (Sigma-Aldrich, D8821), as in previous studies [14,31]. Dextran, promotes aggregation by favoring mainly depletion interactions [14,26,31–33] with a possible contribution of bridging interactions [21]. By varying the dextran concentration from 1 to 5 g/dL, the interaction energy varies in the range $[-5, -1]\ \mu\mathrm{J/m}^2$, as measured by AFM [14,26]. RBCs were introduced in the channel through a flow focusing device that allows us to dilute RBCs with the PBS-dextran solution and focus aggregates around the centerline before they reach the constriction section where further centering is achieved after the first constriction—see the Supplemental Material [29] for a quantification. The flow was controlled by an Elveflow OB1 pressure controller, allowing us to vary extension rates in constrictions between 30 and 650 s^{-1}. The slow velocity of cells in the inlet section ahead of the constrictions allowed for a visual check to ensure that cells had a healthy discocyte shape when entering the channel. The channel had also initially been passivated with a solution of 1 g/L bovine serum albumin (BSA, Sigma-Aldrich, A7906) to prevent undesirable interactions between cells and walls.

Observations were made in bright field microscopy with an Olympus IX71 microscope equipped with a 10× objective lens and a Photron Fastcam Mini-UX100 fast camera (resolution 1.4 pixel/µm). A typical image sequence showing aggregate dissociation is shown in Fig. 1(b). In order to evaluate the actual or effective particle extension rate experienced by aggregates $\dot{\varepsilon} = dv_p/dx$ where v_p is the particle velocity, sequential positions $x(t)$ of a few particles (aggregates) along the hyperbolic constriction were measured and fitted with a function $x(t) = a + b\exp(\dot{\varepsilon}t)$. Note that each aggregate passes through and survives a straight channel with a cross section of 20 µm × 20 µm (where the shear exerted is maximum) before entering the hyperbolic constriction. Hence, any breaking events to the clusters passing through the hyperbolic section must be triggered

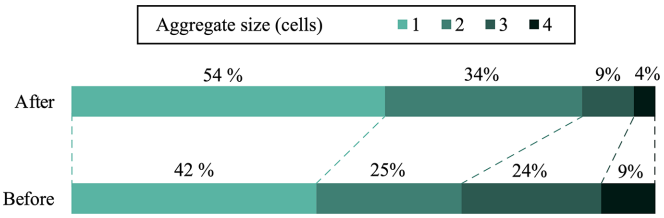

FIG. 2. Distribution of the RBC population in aggregates of different sizes before and after a constriction, for an extension rate $\dot{\varepsilon} = 204\ \mathrm{s}^{-1}$ and a dextran concentration of 3 g/dL.

by the extension rather than shear. This is confirmed by our observation that all breaking events take place significantly before the end of the constriction ($x < 150$ μm), i.e., in a region where shear is much lower compared to the straight section following the previous constriction. Since the only significant difference, in terms of hydrodynamic stresses, between the studied constriction and the straight 20-μm-wide channel located upstream is the additional extensional component, one can safely conclude that aggregate dissociation is controlled by extensional stress in our device and that $\dot{\varepsilon}$ is the relevant parameter.

The evolution of RBC cluster size distribution was evaluated using successively classical image processing and a custom convolutional neural network (CNN) algorithm (see the Supplemental Material [29]). Image processing involves selecting two regions of interest (ROIs) in straight 20-μm-wide sections of the channel located before and after a given constriction in order to compare aggregate size distributions. We verified that no re-aggregation occurs in the abruptly expanding zones after constrictions thanks to the very short residence time of cells. Data sets consisting of images of the two ROIs are then processed by the CNN for classification.

Overall, the image processing allows us to detect and analyze between 1000 and 10 000 objects for a given experiment sequence (fixed flow rate and dextran concentration), which are then classified into single cells, doublets, triplets, quadruplets, and larger objects with respective relative populations S_i, D_i, T_i, Q_i, and N_i [with $i = 0$ before and $i = 1$; see Fig. 1(a)]. These numbers are normalized by the total number of detected RBCs (aggregated or not), such that $S_i + 2D_i + 3T_i + 4Q_i = 1$ (aggregates of five cells or more are very rare and not included in this normalization). An example of the evolution of the distribution of RBCs in aggregates of different sizes (i.e., relative values of S_i, $2D_i$, $3T_i$, and $4Q_i$) when going through the constriction is shown in Fig. 2, reflecting the disaggregation of large aggregates into smaller ones and single cells.

We then define dissociation the probabilities p_d (for doublets), p_t (triplet breaking into a doublet and a single cell), p_{q1} and p_{q2} (quadruplet breaking into respectively two doublets or a single cell and a triplet), with $p_q = p_{q1} + p_{q2}$. Note that based on observation the probability of an aggregate breaking into more than two parts was considered negligible, likely due to stress relaxation when a first bond breaks.

Assuming mass conservation yields the following relations:

$$S_1 = S_0 + 2p_d D_0 + p_t T_0 + p_{q1} Q_0, \tag{1a}$$

$$D_1 = D_0 + p_t T_0 + 2p_{q2} Q_0 - p_d D_0, \tag{1b}$$

$$T_1 = T_0 + p_{q1} Q_0 - p_t T_0, \tag{1c}$$

$$Q_1 = Q_0(1 - p_{q1} - p_{q2}). \tag{1d}$$

This set of linear equations, which is redundant due to mass conservation, can be solved to derive disaggregation probabilities p_d, p_t, and $p_q = p_{q1} + p_{q2}$ by making the additional assumption that the ratio $\lambda = p_{q2}/p_{q1}$ is constant. A sensitivity analysis reveals that the solution of the system of equations only weakly depends on the exact value of λ. Therefore, we made the reasonable assumption that the three different cell-cell bonds in a linear quadruplet had an equal probability of

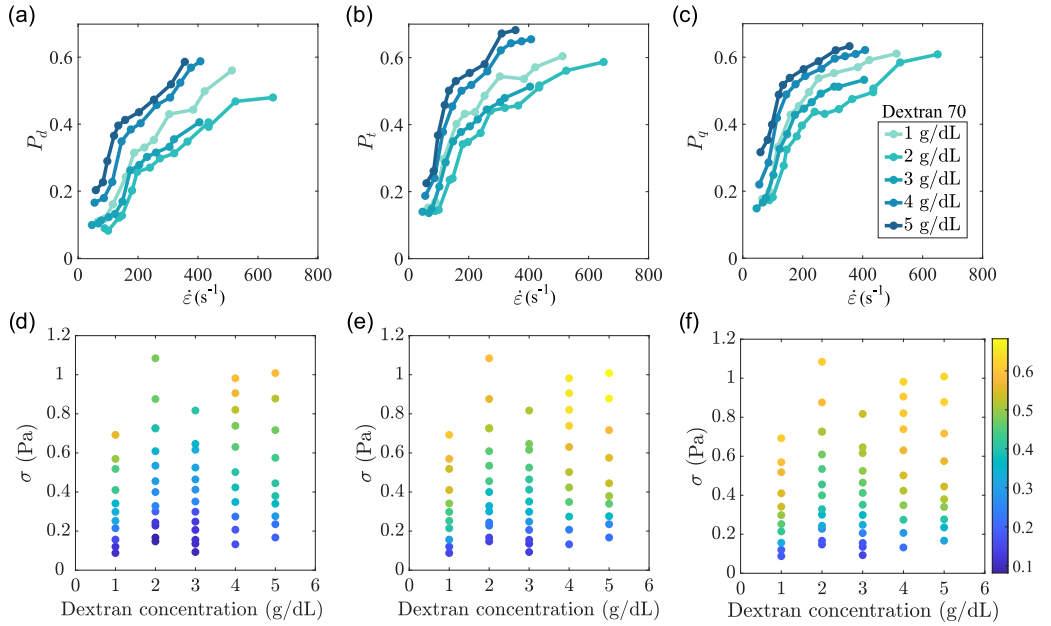

FIG. 3. Aggregate dissociation probabilities as a function of extension rate and dextran 70 kDa concentration. (a)–(c) disaggregation probabilities of doublets (p_d), triplets (p_t), and quadruplets (p_q) vs extension rate $\dot{\varepsilon}$ for different dextran concentrations, showing a sharp transition between 80 and 200 s^{-1}; (d)–(f) disaggregation diagrams in the extension stress $\eta\dot{\varepsilon}$ vs dextran concentration parameter space, respectively, for doublets, triplets, and quadruplets. The color scale represents dissociation probabilities.

breaking, that is, $\lambda = 1/2$. The results are summarized in Fig. 3 where these probabilities are plotted as a function of extension rate and dextran concentration. (See Fig. S5 of the Supplemental Material [29] for comments on sample variability.)

Remarkably, dissociation probabilities show a sigmoid behavior when increasing the extension rate with a strong jump in the range 80–200 s^{-1} that hints at a critical extension rate $\dot{\varepsilon}_c$ and a slower increase at higher extension rates. Ideally, if all aggregates were identical, the same reproducible scenario would apply and they would break at the same extension rate, when flow stresses overcome interaction forces. The dissociation probabilities of Figs. 3(a)–3(c) would then be step functions with zero breaking probability below $\dot{\varepsilon}_c$ and 1 above.

The smoother progression of dissociation probabilities is likely due to several factors. First, the dispersion in orientations and morphologies of aggregates entering the constriction causes variations in aggregate strength and stress. This phenomenon, noted in early studies of aggregate dissociation in shear flow [34], affects dissociation probability. Second, the heterogeneity of cell properties is significant: RBC aging increases stiffness [35–37], impacting aggregation properties [38].

After the transition in the range $80 < \dot{\varepsilon} < 200$ s^{-1}, the dissociation probability increases slowly and neither reaches 1 nor shows asymptotic behavior at the highest rates tested. Doublets, with an aspect ratio close to 1 and less prone to alignment in the flow direction, are particularly robust, with less than 50% dissociating at the highest rate for dextran concentrations of 2–3 g/dl. Although aggregates would eventually break under sufficiently high extension rates and prolonged time, this experimental system cannot vary these factors independently. In the microcirculation, RBC aggregates mainly encounter extensional stresses in bifurcating vessels, making brief periods of extension physiologically significant.

Qualitatively, larger aggregates [Figs. 3(b) and 3(c)] tend to break at slightly lower extension rates than smaller ones, with significantly higher dissociation rates. This is consistent with the higher total

drag force exerted on the surface of longer aggregates, which has to be balanced by attraction force at the weakest cell-cell contact zone in the aggregate.

Figures 3(d)–3(f) display disaggregation diagrams: To account for the non-negligible variation of suspending medium viscosity η with dextran concentration c, we represent disaggregation probabilities in the (σ, c) parameter space where $\sigma = \eta\dot{\varepsilon}$ is the extensional stress. Following previous measurements [32], we take $\eta(c) = -1.78 + 2.84\exp(0.0097c)$ mPa s with c in mg/ml. Interestingly, the dissociation probabilities defined above follow a marked nonmonotonous bell-shaped behavior as in several other RBC aggregation studies with dextran as an aggregation promoter [9,14,31,32]. The comparison of data for doublets, triplets, and quadruplets reveals a consistent pattern wherein the maximum aggregate strength is achieved at dextran concentrations ranging 2–3 g/dl with, again, a global shift towards lower stresses that indicates a higher fragility of larger aggregates.

Assuming a balance between the work of hydrodynamic forces and the interaction energy at the contact zone of two cells, the critical dissociation stress can be estimated through dimensional arguments. For two rounded cells of radius R aligned with the flow, the contact area is a disk with radius R (area $\sim\pi R^2$). In the moving frame at the doublet"s center, it is in a planar elongational flow with extension rate $\dot{\varepsilon}$ and x velocity $\dot{\varepsilon}x$. The average relative fluid velocity with respect to the right cell is $U \sim \dot{\varepsilon}R$ (and $-U$ on the left side), so each cell experiences a drag force similar to the Stokes force on a sphere of radius R,

$$F \sim \pm 6\pi\eta RU \sim \pm 6\pi\eta\dot{\varepsilon}R^2, \tag{2}$$

with a positive sign for the right cell and a negative sign for the left cell. These two opposing forces tend to separate the two cells in the moving frame. Assuming cells are pulled apart a distance δl from the origin of the moving frame, these forces produce a total work

$$W = 2 \times 6\pi\eta\dot{\varepsilon}R^2\delta l. \tag{3}$$

This work compensates the loss of interaction energy between cells. Denoting ϵ_{ad} the interaction energy per unit area as defined earlier [9,14,26,31], the total adhesion energy is

$$E_{ad} = \pi R^2\epsilon_{ad}. \tag{4}$$

By equating $W = E_{ad}$ one gets the critical extension rate required to overcome adhesion:

$$\dot{\varepsilon}_c = \epsilon_{ad}/(12\eta\delta l). \tag{5}$$

Note that in this simple energy balance, we neglected viscous dissipation due to the peeling of RBC membranes from each other. This assumption is based on the large contact angle between membranes resulting from their deformability [see the first snapshots in Fig. 1(b)] and is supported by features of the experimental results: If viscous dissipation between separating membranes were the major force opposing dissociation, the results would be nearly independent of viscosity, extension rate, and interaction energy (see also the Supplemental Material [29] for an estimation of the lubrication-mediated separation timescale).

Taking $\epsilon_{ad} = 5$ μJ/m^2 (maximum value of the interaction energy in dextran 70 kDa solution as measured in Steffen *et al.* [26]), $\eta = 2$ mPa s (approximate viscosity of 3 g/dL dextran solution) and $\delta l \sim 1$ μm (order of magnitude of the displacement required to separate cells), Eq. (5) yields a critical extension rate of order 200 s^{-1} which is the order of magnitude we measured in experiments [Fig. 3(a)].

For larger aggregates (triplets, quadruplets), as the centers of mass of the leftmost and rightmost cells are at a larger distance from the origin of the moving frame, a smaller extension rate is needed to produce the same relative fluid velocity and drag force. Using the same scaling argument, the extension rate required to dissociate an aggregate of N cells becomes

$$\dot{\varepsilon}_c(N) = \dot{\varepsilon}_c/(N/2) = \epsilon_{ad}/(6N\eta\delta l). \tag{6}$$

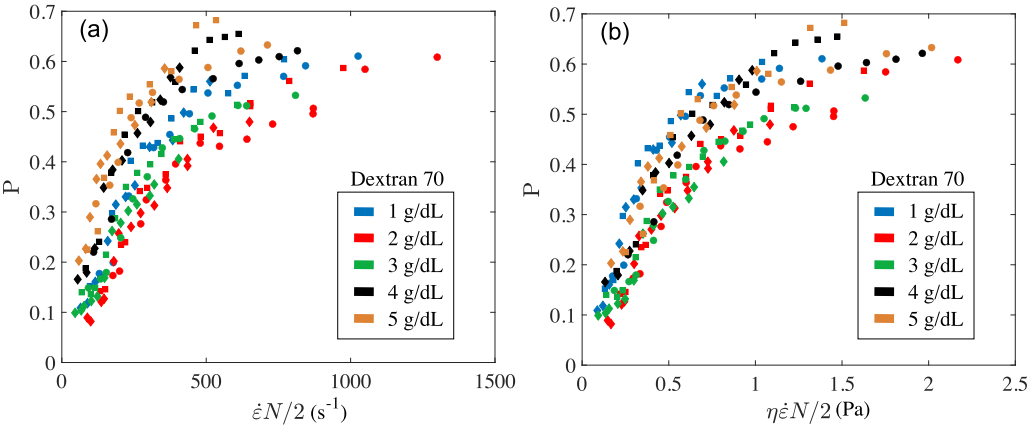

FIG. 4. Aggregate dissociation probability vs $\dot{\epsilon}N/2$ (a) and vs $\eta\dot{\epsilon}N/2$ (b) as suggested by Eq. (6) showing a collapse of data for all aggregate sizes (♦: doublets; ■: triplets; ●: quadruplets) and an ordering from left to right consistent with increasing interaction energy ϵ_{ad}.

This scaling is tested plotting the dissociation probabilities as a function of $\dot{\epsilon}(N/2)$ [Fig. 4(a)] and $\eta\dot{\epsilon}_c N/2$ [Fig. 4(b)], the only independent parameter left being the interaction energy ϵ_{ad}. A nice collapse of experimental data corresponding to different aggregate sizes is obtained in Fig. 4(a), especially considering the initial scattering of individual data series in Figs. 3(a)–3(c), as well as an ordering according to interaction energy in Fig. 4(b) with weak aggregation cases on the left side (1, 4, and 5 g/dL) and a nearly perfect overlap of data for 2 and 3 g/dL consistent with similar values of the adhesion energy near the maximum of the bell-shaped adhesion energy curve [14,26].

Interestingly, the dextran 70-kDa concentration at which the maximum influence of aggregation forces is observed appears highly dependent on experimental setup and stress type: while here we report a maximum resistance to extension at 2–3 g/dL as in AFM measurements [26] or for clusters in straight microchannels [14], other studies reported a peak of aggregation-related phenomena in the range 4–6 g/dL [31,32]. This variation may stem from differences in cell-cell interactions across various flow conditions, potentially leading to shifts in dextran concentration influence.

Conclusion. The response of RBC aggregates to extensional flow stresses was quantitatively investigated by studying dissociation statistics under various levels of stress and interaction forces. This provides an original data set that should be useful for the validation of RBC aggregation models and the benchmarking of numerical simulations. Remarkably, strong changes in behavior are found in a range of parameters corresponding to physiological situations: (i) the range of extension rates, around 100 s^{-1}, where transitions are seen, corresponds to typical extension rates found at bifurcations of the microcirculation *in vivo* (velocities around 1 mm/s in capillaries with diameters around 10 μm) and (ii) considering previously measured values of the interaction energy [14,26], the normal range of physiological fibrinogen concentrations (1.8–4 g/L) corresponds to approximately 1 g/dL of dextran 70 kDa while the concentrations at which we see the most robust aggregates (2–3 g/dL of dextran) correspond to elevated fibrinogen levels seen in pregnancy, inflammatory, and other hyperaggregability cases. This suggests that *in vivo* variations of fibrinogen levels between normal and pathological cases could lead to significant differences in dissociation rates of RBC aggregates in microcirculatory networks and with a likely strong impact on the distribution of aggregate sizes. This is expected to significantly influence the local rheology of blood and hematocrit distribution in capillary networks and calls for further investigations on the behavior of aggregates in complex networks and their impact on blood perfusion.

Finally, the experimental and data analysis principle developed here offer an alternate and relevant way to characterize RBC aggregation that could be used for fundamental studies on the

influence of RBC mechanical properties, aggregation mechanisms (using different aggregation promoters such as fibrinogen or pure depletant agents [39]), or for an improved evaluation of the aggregability of healthy and pathological blood samples in clinical contexts.

Acknowledgments. We thank M. Van Melle-Gateau (LIPhy, CNRS-UGA) for microfabrication, J. Martin-Wortham for experimental advice, and M. Karrouch for technical support. T.P. thanks G. Ghigliotti, G. Coupier, F. Yaya, C. Boucly, and C. Wagner for discussions. This work was supported by CNES (Centre National d'Etudes Spatiales, DAR ID 8106 "Rhéologie sanguine"). The authors are members of LabEx Tec21 (Investissements d'Avenir Grant Agreement No. ANR-11-LABX-0030).

[1] O. Baskurt, B. Neu, and H. J. Meiselman, *Red Blood Cell Aggregation* (CRC, Boca Raton, 2011).

[2] S. Chien, Shear dependence of effective cell volume as a determinant of blood viscosity, Science **168**, 977 (1970).

[3] S. E. Bedell and B. T. Bush, Erythrocyte sedimentation-rate - from folklore to facts, Am. J. Med. **78**, 1001 (1985).

[4] S. Chien and K.-M. Jan, Red cell aggregation by macromolecules: Roles of surface adsorption and electrostatic repulsion, J. Supramol. Struct. **1**, 385 (1973).

[5] P. Bagchi, P. C. Johnson, and A. S. Popel, Computational fluid dynamic simulation of aggregation of deformable cells in a shear flow, J. Biomech. Eng. **127** 1070 (2005).

[6] D. Lominadze and W. L. Dean, Involvement of fibrinogen specific binding in erythrocyte aggregation, FEBS Lett. **517**, 41 (2002).

[7] Y. V. Pereverzev, O. V. Prezhdo, M. Forero, E. V. Sokurenko, and W. E. Thomas, The two-pathway model for the catch-slip transition in biological adhesion, Biophys. J. **89**, 1446 (2005).

[8] S. Asakura and F. Oosawa, Interaction between particles suspended in solutions of macromolecules, J. Polym. Sci. **33**, 183 (1958).

[9] B. Neu and H. J. Meiselman, Depletion-mediated red blood cell aggregation in polymer solutions, Biophys. J. **83**, 2482 (2002).

[10] A. M. Robertson, A. Sequeira, and M. V. Kameneva, Hemodynamical Flows Modeling, Analysis and Simulation, *Hemorheology* (Birkhäuser Basel, Basel, 2008), pp. 63–120.

[11] T. Podgorski, Biological Flow in Large Vessels, *Hemodynamics and Hemorheology* (John Wiley and Sons Ltd, 2022), Chap.1, pp. 1–41.

[12] J. J. Bishop, P. R. Nance, A. S. Popel, M. Intaglietta, and P. C. Johnson, Effect of erythrocyte aggregation on velocity profiles in venules, Am. J. Physiol.: Heart Circulatory Physiol. **280**, H222 (2001).

[13] J. Zhang, P. C. Johnson, and A. S. Popel, Effects of erythrocyte deformability and aggregation on the cell free layer and apparent viscosity of microscopic blood flows, Microvasc. Res. **77**, 265 (2009).

[14] M. Brust, O. Aouane, M. Thiébaud, D. Flormann, C. Verdier, L. Kaestner, M. Laschke, H. Selmi, A. Benyoussef, T. Podgorski, G. Coupier, C. Misbah, and C. Wagner, The plasma protein fibrinogen stabilizes clusters of red blood cells in microcapillary flows, Sci. Rep. **4**, 4348 (2014).

[15] W. H. Reinhart, N. Z. Piety, and S. S. Shevkoplyas, Influence of red blood cell aggregation on perfusion of an artificial microvascular network, Microcirculation **24**, e12317 (2017).

[16] B. M. Fenton, R. T. Carr, and G. R. Cokelet, Nonuniform red cell distribution in 20 to 100 μm bifurcations, Microvasc. Res. **29**, 103 (1985).

[17] V. Doyeux, T. Podgorski, S. Peponas, M. Ismail, and G. Coupier, Spheres in the vicinity of a bifurcation: Elucidating the zweifach–fung effect, J. Fluid Mech. **674**, 359 (2011).

[18] Z. Shen, G. Coupier, B. Kaoui, B. Polack, J. Harting, C. Misbah, and T. Podgorski, Inversion of hematocrit partition at microfluidic bifurcations, Microvasc. Res. **105**, 40 (2016).

[19] J. M. Sherwood, E. Kaliviotis, J. Dusting, and S. Balabani, Hematocrit, viscosity and velocity distributions

of aggregating and non-aggregating blood in a bifurcating microchannel, Biomech. Model. Mechanobiol. **13**, 259 (2014).

[20] E. Kaliviotis, J. M. Sherwood, and S. Balabani, Partitioning of red blood cell aggregates in bifurcating microscale flows, Sci. Rep. **7**, 44563 (2017).

[21] F. Yaya, Physical properties of red blood cells in aggregation, Theses, Université Grenoble Alpes; Universität des Saarlandes, 2021.

[22] V. Clavería, O. Aouane, M. Thiébaud, M. Abkarian, G. Coupier, C. Misbah, T. John, and C. Wagner, Clusters of red blood cells in microcapillary flow: Hydrodynamic versus macromolecule induced interaction, Soft Matter **12**, 8235 (2016).

[23] A. R. Pries, T. W. Secomb, and P. Gaehtgens, Structure and hemodynamics of microvascular networks - heterogeneity and correlations, Am. J. Physiol.: Heart Circulatory Physiol. **269**, H1713 (1995).

[24] J. Zhang, P. C. Johnson, and A. S. Popel, Red blood cell aggregation and dissociation in shear flows simulated by lattice Boltzmann method, J. Biomech. **41**, 47 (2008).

[25] D. A. Fedosov, W. Pan, B. Caswell, G. Gompper, and G. E. Karniadakis, Predicting human blood viscosity in silico, Proc. Natl. Acad. Sci. USA **108**, 11772 (2011).

[26] P. Steffen, C. Verdier, and C. Wagner, Quantification of depletion-induced adhesion of red blood cells, Phys. Rev. Lett. **110**, 018102 (2013).

[27] D. Bento, R. O. Rodrigues, V. Faustino, D. Pinho, C. S. Fernandes, A. I. Pereira, V. Garcia, J. M. Miranda, and R. Lima, Deformation of red blood cells, air bubbles, and droplets in microfluidic devices: Flow visualizations and measurements, Micromachines **9**, 151 (2018).

[28] V. Faustino, R. O. Rodrigues, D. Pinho, E. Costa, A. Santos-Silva, V. Miranda, J. S. Amaral, and R. Lima, A microfluidic deformability assessment of pathological red blood cells flowing in a hyperbolic converging microchannel, Micromachines **10**, 645 (2019).

[29] See Supplemental Material at http://link.aps.org/supplemental/10.1103/PhysRevFluids.9.L071101, which includes Refs. [40–45] for COMSOL flow simulation results, a quantification of cell focusing, a description of the Convolutional Neural Network, an assessment of the variability of results between blood samples, and an estimation of the influence of lubrication effects in the separation process.

[30] A. Merlo, S. Losserand, F. Yaya, P. Connes, M. Faivre, S. Lorthois, C. Minetti, E. Nader, T. Podgorski, C. Renoux, G. Coupier, and E. Franceschini, Influence of storage and buffer composition on the mechanical behavior of flowing red blood cells, Biophys. J. **122**, 360 (2023).

[31] D. Flormann, O. Aouane, L. Kaestner, C. Ruloff, C. Misbah, T. Podgorski, and C. Wagner, The buckling instability of aggregating red blood cells, Sci. Rep. **7**, 7928 (2017).

[32] D. Flormann, K. Schirra, T. Podgorski, and C. Wagner, On the rheology of red blood cell suspensions with different amounts of dextran: Separating the effect of aggregation and increase in viscosity of the suspending phase, Rheol. Acta **55**, 477 (2016).

[33] F. Yaya, J. Roemer, A. Guckenberger, T. John, S. Gekle, T. Podgorski, and C. Wagner, Vortical flow structures induced by red blood cells in capillaries, Microcirculation **28**, e12693 (2021).

[34] R. Skalak, Aggregation and disaggregation of red blood cells, Biorheology **21**, 463 (1984).

[35] R. E. Waugh, M. Narla, C. W. Jackson, T. J. Mueller, T. Suzuki, and G. L. Dale, Rheologic properties of senescent erythrocytes: Loss of surface area and volume with red blood cell age, Blood **79**, 1351 (1992).

[36] F. H. Bosch, J. M. Werre, L. Schipper, B. Roerdinkholder-Stoelwinder, T. Huls, F. L. A. Willekens, G. Wichers, and M. R. Halie, Determinants of red blood cell deformability in relation to cell age, Eur. J. Haematology **52**, 35 (1994).

[37] R. S. Franco, M. R. Puchulu-Campanella, L. A. Barber, M. B. Palascak, C. H. Joiner, P. S. Low, and R. M. Cohen, Changes in the properties of normal human red blood cells during in vivo aging, Am. J. Hematol. **88**, 44 (2013).

[38] M. Hoore, F. Yaya, T. Podgorski, C. Wagner, G. Gompper, and D. A. Fedosov, Effect of spectrin network elasticity on the shapes of erythrocyte doublets, Soft Matter **14**, 6278 (2018).

[39] O. Korculanin, T. Kochetkova, and M. P. Lettinga, Competition between red blood cell aggregation and breakup: Depletion force due to filamentous viruses vs shear flow, Front. Phys. **9**, 721368 (2021).

[40] S. Losserand, G. Coupier, and T. Podgorski, Migration velocity of red blood cells in microchannels, Microvasc. Res. **124**, 30 (2019).

[41] V. Vitkova, M.-A. Mader, and T. Podgorski, Deformation of vesicles flowing through capillaries, Europhys. Lett. **68**, 398 (2004).

[42] G. Hetsroni, S. Haber, and E. Wacholder, The flow fields in and around a droplet moving axially within a tube, J. Fluid Mech. **41**, 689 (1970).

[43] M. Abadi, P. Barham, J. Chen, Z. Chen, A. Davis, J. Dean, M. Devin, S. Ghemawat, G. Irving, M. Isard, M. Kudlur, J. Levenberg, R. Monga, S. Moore, D. G. Murray, B. Steiner, P. Tucker, V. Vasudevan, P. Warden, M. Wicke, Y. Yu, and X. Zheng, Tensorflow: A system for large-scale machine learning, in *Proceedings of the OSDI'16: 12Th Usenix Symposium on Operating Systems Design and Implementation* (USENIX Assoc, Savannah, GA, 2016), pp. 265–283.

[44] P. Ermolinskiy, A. Lugovtsov, F. Yaya, K. Lee, L. Kaestner, C. Wagner, and A. Priezzhev, Effect of red blood cell aging in vivo on their aggregation properties in vitro: Measurements with laser tweezers, Appl. Sci. **10**, 7581 (2020).

[45] S. Chien, Bioelectrochemistry: Ions, Surfaces, Membranes, *Aggregation of Red Blood Cells: An Electrochemical and Colloid Chemical Problem*, Advances in Chemistry (American Chemical Society, 1980), Vol. 188, pp. 3–38.